*JOURNAL OF NANO- AND ELECTRONIC PHYSICS*
Vol. **18** No 3, 03037(6pp) (2026)

*ЖУРНАЛ НАНО- ТА ЕЛЕКТРОННОЇ ФІЗИКИ*
Том **18** № 3, 03037(6cc) (2026)

OPEN ACCESS

**REGULAR ARTICLE**

# High-Quality Electrical Conductivity $Co_3S_4$ Thin Films Prepared by Spray Pyrolysis

Abdelouahab Gahtar[1], Laid Dahbi[2], Chouaieb Zaouche[2], Said Benramache[3,*], Amira Sbaihi[3], Abdelghani Lakel[3], Okba Belahssen[3]

[1] *Department of Biology, Faculty of Sciences, University Elchahid Hamma Lakhder, 39000 El Oued, Algeria*
[2] *SALAMA Lab, Higher School of Saharan Agriculture – El Oued, PB 90 Chouhada, 39011 El-Oued, Algeria*
[3] *Laboratoire des Matériaux, des Énergies et de l'Environnement, University of Biskra 07000, Algeria*

(Received 25 March 2026; revised manuscript received 23 June 2026; published online 26 June 2026)

This study reports the deposition of cobalt sulfide ($Co_3S_4$) thin films on glass substrates using the spray pyrolysis technique at a substrate temperature of 350 ± 5 °C. The precursor solution was prepared from cobalt chloride hexahydrate and thiourea dissolved in bidistilled water, while a small amount of acetic acid was added to enhance the solubility and stability of the solution. The structural properties of the deposited films were investigated using X-ray diffraction analysis, which confirmed the formation of polycrystalline $Co_3S_4$ with a cubic spinel structure (Fd-3m). The films exhibited a preferred orientation along the (113) crystallographic plane. The average crystallite size was found to be approximately 13.4 nm, with a calculated lattice parameter of 9.405 Å, indicating good crystalline quality. Optical characterization revealed that the films possess a direct optical band gap of 1.88 eV, suggesting strong absorption in the visible region, which is advantageous for optoelectronic applications. FTIR spectroscopy confirmed the presence of characteristic Co-S bonding vibrations, verifying successful sulfide formation. Electrical measurements showed a high electrical conductivity of about $9.60 \times 10^4$ $(\Omega \cdot cm)^{-1}$, indicating quasi-metallic behavior and efficient charge transport within the film. These combined structural, optical, and electrical properties demonstrate that spray pyrolysis is a simple, low-cost, and effective method for producing high-quality $Co_3S_4$ thin films, making them promising candidates for applications in optoelectronic devices, sensors, and energy-related technologies.

**Keywords:** Cobalt sulfide, Spray pyrolysis, XRD, FTIR, Electrical conductivity.

DOI: 10.21272/jnep.18(3).03037 PACS numbers: 73.61.Jc, 82.30.Lp

## 1. INTRODUCTION

Cobalt sulfide-based materials have attracted significant attention due to their tunable electronic structure, diverse phases, and multifunctional properties suitable for energy storage and conversion applications [1-3]. The multiple oxidation states of cobalt enable precise control of optical, electrical, and electrochemical characteristics, making these compounds promising for supercapacitors, electrocatalysis, and battery technologies [4,5].

Recent studies have highlighted that $Co_3S_4$ nanostructures and thin films exhibit high electrical conductivity, favorable band gaps, and significant electrochemical activity, which are desirable for optoelectronic and photovoltaic applications [3, 6]. However, achieving phase-controlled, uniform, and highly conductive films using cost-effective and scalable techniques remains a challenge. Methods involving complex vacuum systems or multi-step processes are limited in large-area production [7].

Spray pyrolysis has emerged as a simple and reproducible technique for thin-film fabrication. It allows control over film composition and microstructure while avoiding toxic reagents, making it suitable for industrial applications [8]. Despite its potential, systematic studies correlating the structural phase of $Co_3S_4$ films with their optical and electrical properties are still limited [3, 8].

In this work, we investigate the controlled deposition of $Co_3S_4$ thin films on glass substrates using spray pyrolysis. The focus is on elucidating the structure-property relationships through detailed analysis of their structural, optical, and electrical characteristics, providing insights for advanced energy and optoelectronic applications.

## 2. EXPERIMENTAL DETAILS

### 2.1 2.1. Deposition of $Co_3S_4$ Thin Films

Cobalt sulfide ($Co_3S_4$) thin films were prepared on glass substrates using the spray pyrolysis technique. The precursor solution was obtained by dissolving cobalt chloride hexahydrate ($CoCl_3 \cdot 6H_2O$) and thiourea ($CS(NH_4)_2$) in 100 mL of deionized water under stirring at 70 °C. A few drops of hydrochloric acid (HCl) were added to ensure complete dissolution of the precursors. Films were deposited at a substrate temperature of 350 °C, with a 10 cm distance maintained between the spray nozzle and the substrate. Ambient air served as the carrier gas at a flow rate of 2 mL/min. After deposition, the films were allowed to cool naturally to room

* Correspondence e-mail: s.benramache@univ-biskra.dz





Cite this article as: A. Gahtar et al., *J. Nano- Electron. Phys.* 18 No 3, 03037 (2026) https://doi.org/10.21272/jnep.18(3).03037

temperature. The film thickness was determined using the gravimetric (weight difference) method according to the relation (1) [9]:

$$d = \frac{m}{\rho * S} \quad (1)$$

where $e$ represents the film thickness, $m$ is the mass of material deposited on the substrate, $S$ denotes the coated area, and $\rho$ is the density of cobalt sulfide, taken as 5.45 g $cm^{-3}$ [10]. Based on this method, the average film thickness was estimated to be approximately 527 nm.

### 2.2 Characterization Techniques

Structural analysis was conducted using X-ray diffraction (XRD, Mini Flex-Rigaku) with Cu-Kα radiation ($\lambda$ = 1.5418 Å) over the 2$\theta$ range of 20-60°. Optical properties were examined using a dual-beam UV-visible spectrophotometer (UV-3101, Shimadzu) from 300-1100 nm. Electrical conductivity was measured using a four-point probe technique with evaporated gold contacts on the film surface. FTIR spectroscopy (Shimadzu IR Affinity-1) was employed to analyze the chemical bonding within the thin films in the range of 400-4000 $cm^{-1}$. All characterizations were performed without post-deposition thermal treatment.

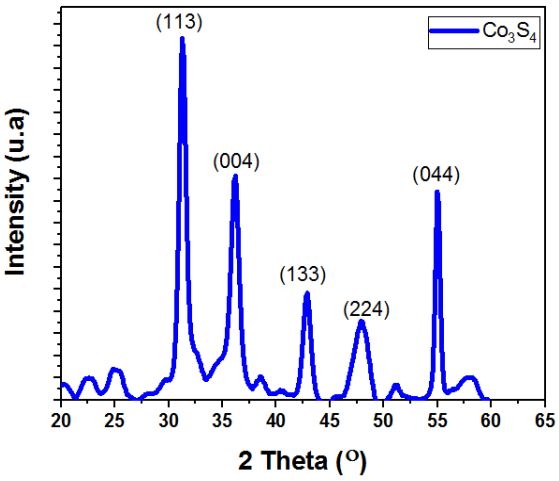


**Fig. 1** – X-ray diffraction (XRD) pattern of the $Co_3S_4$ thin film

## 3. RESULTS AND DISCUSSION

### 3.1 X-Ray Diffraction

The primary objective of this investigation was to examine the structural properties of cobalt sulfide thin films deposited at a substrate temperature of 350 °C. The crystalline structure was analyzed by X-ray diffraction, where the diffraction patterns were collected in the 2$\theta$ range of 20-60° using Cu Kα radiation with a wavelength of 1.5406 Å. The XRD measurements were performed under an accelerating voltage of 40 kV and a tube current of 40 mA. The obtained diffraction patterns are presented in Figure 1

Figure 1 illustrates the X-ray diffraction pattern of $Co_3S_4$ thin films deposited using the spray pyrolysis method. The diffraction peaks clearly indicate that the synthesized film possesses a polycrystalline nature and crystallizes in a cubic structure indexed to the Fd-3m space group (No 227). A pronounced preferential growth along the (113) crystallographic plane is evident, as reflected by the significantly higher intensity of this peak compared to those corresponding to the (004), (133), (224), and (044) planes. The observed diffraction peaks were successfully indexed using the standard JCPDS card No. 01-073-1703, confirming the formation of the $Co_3S_4$ phase without detectable secondary phases. Furthermore, the structural features obtained in the present work are consistent with previously reported results for $Co_3S_4$ thin films synthesized via spray pyrolysis as well as other deposition techniques, indicating good reproducibility and phase stability of the material [2,6,10].

To further evaluate the preferred crystallographic orientation, the texture coefficient ($TC_{hkl}$) was calculated based on the relative intensities of the diffraction peaks ($I_{hkl}$). This parameter provides insight into the degree of orientation preference and the likelihood of crystal growth along a specific ($hkl$) direction. The texture coefficient was determined using the following expression (2) [11].

$$TC(hkl) = \frac{I_{hkl} / I_{0hkl}}{N^{-1} \sum_n I_{hkl} / I_{0hkl}} \quad (2)$$

where $I_{0hkl}$ represents the standard diffraction intensity corresponding to the ($hkl$) plane taken from the JCPDS reference file, and $N$ denotes the total number of diffraction peaks considered in the analysis. The calculated texture coefficient values are summarized in Table 1. The results clearly show that the (113) reflection exhibits the highest texture coefficient among all observed planes, indicating a strong preferential growth along this crystallographic direction. Consequently, the (113) peak appears with the maximum diffraction intensity relative to the other reflections.

In addition, the average crystallite size ($D$) was evaluated for the prominent diffraction peaks using the Debye-Scherrer equation (3) [12]

$$G_{hkl} = \frac{k\lambda}{\beta \cos\theta} \quad (3)$$

In this expression, $k$ is the shape factor, taken as 0.90, $\beta$1/2 represents the full width at half maximum (FWHM) of the respective diffraction peak, $\theta$ corresponds to the Bragg angle for each ($hkl$) plane, and $\lambda$ = 1.5406 Å denotes the wavelength of the Cu Kα X-ray radiation employed in the measurements.

**Table 1** – Calculated values of texture coefficients ($TC_{hkl}$), crystallite sizes ($D_{hkl}$), residual stresses ($\varepsilon_{hkl}$), and dislocation densities ($\delta_{hkl}$) for the deposited $Co_3S_4$ thin films

| $hkl$ | $TC_{hkl}$ | $G_{hkl}$ (nm) | $\delta_{hkl}$ ($10^{15}$ lines/$m^2$) | $\varepsilon_{hkl}$ ($10^{-3}$) |
|---|---|---|---|---|
| 113 | 1.501 | 16.904 | 3.502 | 8.637 |
| 004 | 0.418 | 15.098 | 4.387 | 7.443 |
| 133 | 0.923 | 10.277 | 9.468 | 9.218 |
| 422 | 0.917 | 10.469 | 9.123 | 8.192 |
| 440 | 1.488 | 14.195 | 4.812 | 4.637 |

Additionally, the residual stress ($\varepsilon_{hkl}$) and dislocation density ($\delta_{hkl}$) within the films were calculated using the following relations [13]

$$\begin{cases} \delta_{hkl} = \dfrac{1}{G^2{}_{hkl}} \\ \varepsilon_{hkl} = \dfrac{\beta}{4\tan\theta} \end{cases} \quad (4)$$

Moreover, the average crystallite size, microstrain and dislocation density of the films can be estimated by incorporating the texture coefficients, following the mathematical relations reported in reference [11-13]

$$\begin{cases} \langle G \rangle = \dfrac{\sum G_{hkl}}{5} \\ \langle \delta \rangle = \dfrac{\sum \delta_{hkl}}{5} \\ \langle \varepsilon \rangle = \dfrac{\sum \varepsilon_{hkl}}{5} \end{cases} \quad (5)$$

The average dislocation density, microstrain, and crystallite size were determined to be $7.625 \times 10^{15}$ lines/nm$^2$, $6.258 \times 10^{-3}$, and 13.388 nm, respectively. These values indicate the formation of a high-quality thin film. During the crystallization process, dislocations acquire sufficient energy to become mobile, allowing them to migrate toward grain boundaries. As the crystallization proceeds, these activated dislocations redistribute and are effectively neutralized, contributing to the structural stability of the film.

### 3.2 Optical Properties

Figure 2 presents the transmission and absorbance spectra of the $Co_3S_4$ thin films measured at room temperature. It can be seen that both transmittance and absorbance decrease significantly in the ultraviolet region. Above 400 nm, the films exhibit increased optical transparency, which can be attributed to reduce light scattering and minimized propagation losses. The average optical transmittance and absorbance were found to be approximately 0.77 % and 2.16 arbitrary units, respectively. Additionally, the lack of interference fringes at longer wavelengths is primarily associated with surface roughness in the deposited films.

The absorption coefficient ($\alpha$) of the $Co_3S_4$ thin films was determined from the measured transmittance and reflectance spectra using the expression given in equation (9) [14].

$$\alpha = \frac{1}{e}\ln\left(\frac{1}{T}\right) \quad (6)$$

In this relation, $d$ represents the film thickness and $T$ is the measured transmittance. Figure 3 illustrates the dependence of the absorption coefficient ($\alpha$) on the wavelength ($\lambda$). The average absorption coefficient was calculated to be approximately $7.284 \times 10^4$ cm$^{-1}$, which falls within the typical range reported for semiconducting thin films. This value is also consistent with previously published data for similar semiconducting reflective films [14].

For high photon energies ($h\upsilon$), the absorption coefficient ($\alpha$) of the studied films follows the relationship described in reference [15]:

$$\alpha h\upsilon = B\left(h\upsilon - E_g\right)^p \quad (7)$$

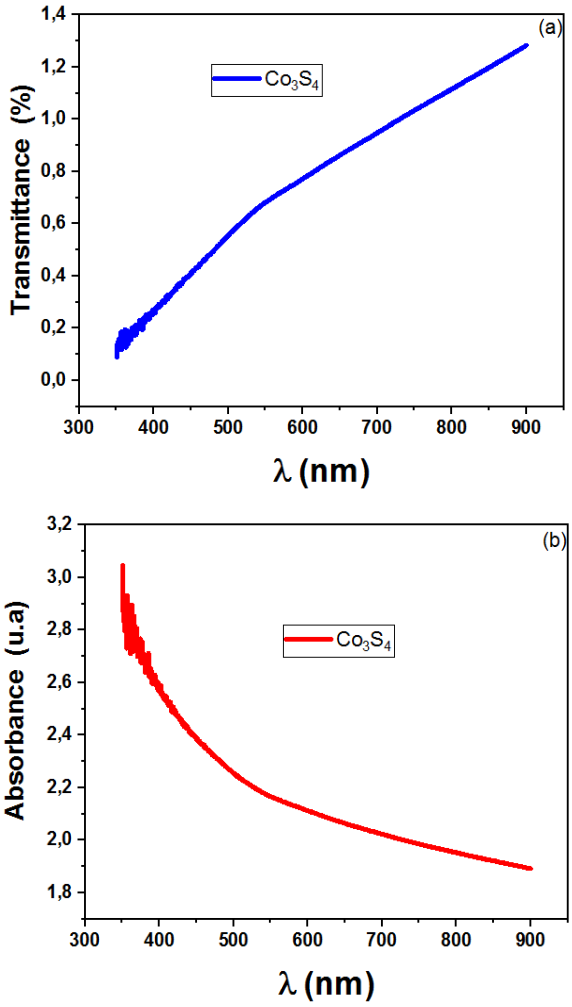


**Fig. 2** – UV-visible spectra of $Co_3S_4$ thin films showing (a) optical transmittance and (b) absorbance measured at room temperature

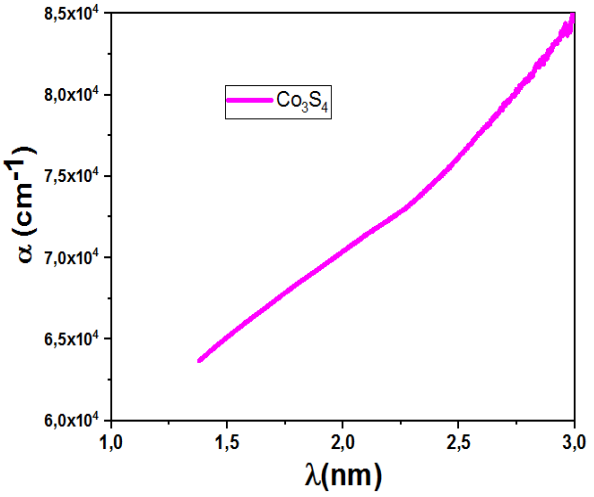


**Fig. 3** – Variation of the absorption coefficient ($\alpha$) of the $Co_3S_4$ thin films as a function of wavelength

In this expression, $B$ is a constant, and $p$ is an integer representing the type of electronic transition, taking the value 1/2 for direct transitions and 2 for indirect transitions. Figure 4 presents the $(\alpha h\upsilon)^2$ versus photon energy ($h\upsilon$) plots for $Co_3S_4$ thin films deposited on glass substrates via the spray pyrolysis technique at a substrate temperature of 350 °C.

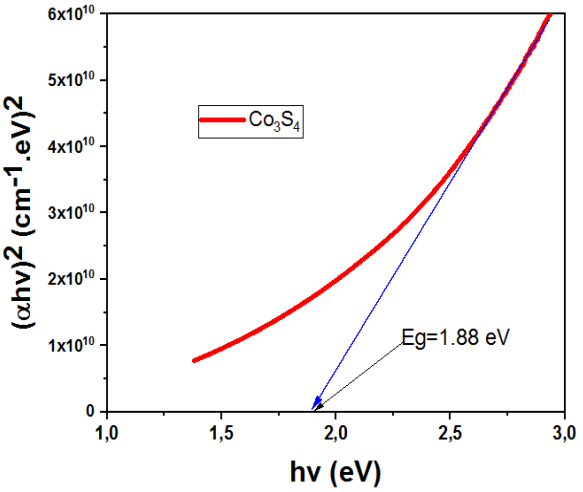


**Fig. 4** – Plot of $(\alpha h\upsilon)^2$ as a function of photon energy ($h\upsilon$) for the nanostructured $Co_3S_4$ thin films

By linearly extrapolating the $(\alpha h\upsilon)^2$ versus $h\upsilon$ plot, the intersection with the energy axis corresponds to the optical transition energy. The optical band gap of the $Co_3S_4$ thin films was determined to be 1.88 eV, which is consistent with previously reported values in the literature [14, 15]. This value also aligns with the structural characterization, exhibiting a blue shift relative to the bulk material, which has a band gap of approximately 0.8 eV. The observed shift of ~ 245 meV can be attributed to quantum confinement effects combined with the Moss-Burstein phenomenon. Consequently, additional energy is required for electronic transitions due to both the filling of the conduction band edges and the reduction in particle size.

### 3.3 Electrical Properties

The sheet (or surface) resistance of the thin films was determined using a four-point probe technique [16]. In this method, four collinearly arranged metallic contacts are placed on the central region of the sample. A small current ($I$) is applied through the two outer contacts, while the voltage ($V$) is measured across the two inner contacts. The measured V/I ratio is then multiplied by a correction factor ($K$) to account for the finite dimensions of the sample. Using this approach, the electrical conductivity of the $Co_3S_4$ films was calculated based on the experimentally determined sheet resistance according to the following relation [16]:

$$\begin{cases} R_{sh} = \dfrac{\pi}{\ln 2}\dfrac{V}{I} \\ \sigma = \dfrac{1}{\rho} = \dfrac{1}{eR_{sh}} \end{cases} \quad (8)$$

In this expression, $\rho$ represents the electrical resistivity, $e$ is the film thickness, $I$ is the applied current (1 nA), and $V$ is the measured voltage. The results of the electrical characterization for the $Co_3S_4$ thin films are summarized in Table 2.

**Table 2** – Electrical properties of the $Co_3S_4$ thin films, including resistivity, sheet resistance, and conductivity

| Thin film | Film thickness $e$ (nm) | Sheet resistance $R_{sh}$ (Ω·cm) | Electrical resistivity $\rho$ (Ω·cm) | Electrical conductivity $\sigma$ (Ω·cm)$^{-1}$ |
|---|---|---|---|---|
| $Co_3S_4$ | 527.128 | $1.97 \times 10^{-1}$ | $1.04 \times 10^{-5}$ | $9.60 \times 10^{4}$ |

Table 2 shows that the $Co_3S_4$ thin films exhibit a high electrical conductivity of approximately $9.60 \times 10^4$ (Ω·cm)$^{-1}$, indicating a semi-metallic behavior for the deposited layer. These findings are consistent with previously reported values in the literature [15, 16]. Cobalt (II, III) sulfide ($Co_3S_4$) is a mixed-valence compound composed of $Co^{+2}$ and $Co^{+3}$ ions, which contributes to its notable electrical properties. The electrical conductivity of $Co_3S_4$ is influenced by factors such as temperature, crystalline structure, and the presence of impurities or defects. Enhancing the conductivity can be achieved by introducing dopants or creating controlled defects in the lattice. For instance, doping with transition metals like iron (Fe) or nickel (Ni) has been demonstrated to improve the charge transport properties of $Co_3S_4$ thin films.

### 3.4 FTIR Analysis

Fourier-transform infrared (FTIR) spectroscopy provides precise information about the molecular structure of both organic and inorganic constituents. The FTIR spectra of the $Co_3S_4$ thin films deposited at a substrate temperature of 350 °C are presented in Figure 5.

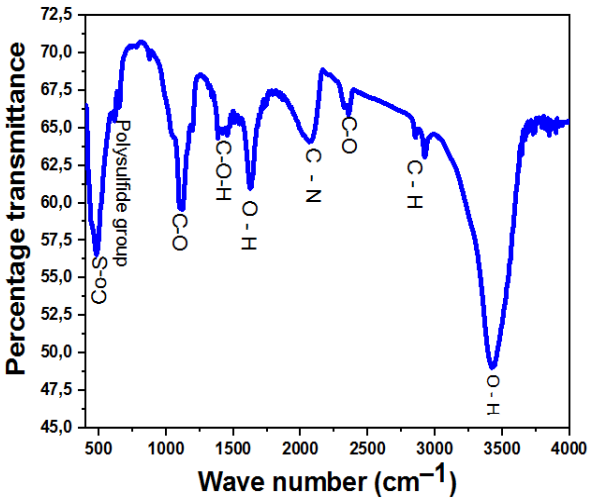


**Fig. 5** – FTIR spectra of the nanostructured $Co_3S_4$ thin films, showing the characteristic vibrational modes of the material

The $Co_3S_4$ thin film deposited over 3.5 hours exhibits five prominent absorption bands at 3202 cm$^{-1}$, 1560 cm$^{-1}$, 1428 cm$^{-1}$, 1068 cm$^{-1}$, and 3209 cm$^{-1}$. The bands near 3200 cm$^{-1}$ and 1638 cm$^{-1}$ are attributed to the stretching and bending vibrations of –OH groups, likely originating from adsorbed water molecules [17]. Absorption bands at 1428 cm$^{-1}$ and 1067-1068 cm$^{-1}$

correspond to C–O–H and C–O stretching vibrations, which may arise either from residual carbon in the precursors or from atmospheric $CO_2$ [18]. The peak observed at 607 $cm^{-1}$ is characteristic of Co–S stretching vibrations and polysulfide bond formations [18,19]. Additionally, the strong bands around 1067-1068 $cm^{-1}$ are associated with bending vibrations of sulfonated groups present in CoS, $Co_2S_2$, and $Co_3S_4$ phases [19,20]. These spectral features confirm the presence of cobalt-sulfur bonding in the deposited films while also revealing minor contributions from hydroxyl and carbon-containing groups.

## 4. CONCLUSION

High-quality $Co_3S_4$ thin films were successfully fabricated on glass substrates using the spray pyrolysis technique, as verified by X-ray diffraction (XRD) analysis. The method provides notable advantages, such as simplicity, low cost, ease of operation, and relatively low deposition temperatures. In this work, the films were deposited at 325 °C without applying any post-deposition thermal treatment. Morphological studies revealed that the films possess a smooth, dense, and granular surface, while XRD analysis confirmed their polycrystalline cubic structure with a preferential orientation along the (113) plane. The average crystallite size was approximately 14.95 nm. Optical characterization indicated a metallic-like response, with an average visible transmittance of 1.10 % and a direct band gap of 1.88 eV. Furthermore, electrical measurements showed a high conductivity of $9.60 \times 10^4$ Ω·cm at room temperature.

Overall, these results demonstrate that the synthesized $Co_3S_4$ thin films combine excellent structural quality with remarkable electrical properties, making them promising candidates for applications in electrocatalysis, microelectronic devices, rechargeable batteries, and as metal barrier or liner layers.

## REFERENCES


1. T. Liu, J. Li, H. Cui, Y. Liu, K. Liu, H. Wei, M. Wang, *J Energy Chem*. **76**, 339 (2023) https://doi.org/10.1016/j.jechem.2022.10.012.
2. S.A. Boussaa, L. Talbi, K. Benfadel, et al., *J. Mater. Res.* **40**, 727 (2025) https://doi.org/10.1557/s43578-025-01531-9.
3. O. Samperi, L. Vines, M.P. Bertolini, M. Cantiano, S. Coffa, M.El. Fragalà, *Mater. Sci. Semicond. Process*. **174**, 108219 (2024) https://doi.org/10.1016/j.mssp.2024.108219.
4. X. Wang, W. Yu, M. Wang, F. Wang, B. Yang, *Mater. Chem. Phys*. **308**, 128295 (2023). https://doi.org/10.1016/j.matchemphys.2023.128295.
5. Y. Dou, Z. Liu, L. Zhao, et al., *Nano-Micro Lett.* **18**, 51 (2026) https://doi.org/10.1007/s40820-025-01895-x.
6. K. Yu, Z. Jiang, L. Liu, et al., *Ionics* **32**, 5783 (2026) https://doi.org/10.1007/s11581-026-07128-4.
7. A. Majid, U. Najam, S. Ahmad, M. Alkhedher, *Mater. Sci. Semicond. Process*. **176**, 108320 (2024) https://doi.org/10.1016/j.mssp.2024.108320.
8. A. Gahtar, C. Zaouche, A. Ammari, L. Dahbi, *Chalcogenide Lett*. **20** No 5, 377 (2023) https://doi.org/10.15251/CL.2023.205.377.
9. F. Harrathi, E. Aubry, S. Dridi, P. Briois, N. Bitri, *J. Mater. Sci.: Mater. Electron*. **34** No 4, 304 (2023) https://doi.org/10.1007/s10854-022-09720-6.
10. A. Gahtar, A. Benali, S. Benramache, C Zaouche, *Chalcogenide Lett*. **19** No 2, 103 (2022) https://doi.org/10.15251/CL.2022.192.103.
11. J.O. Emegha, et al., *Chem. Inorg. Mater.* **4**, 100068 (2024) https://doi.org/10.1016/j.cinorg.2024.100068.
12. Y. Pengfei, S. Lili, H. Xiangyu, X. Chuanhui, W. Haiying, W. Feng, *Rare Met. Mater. Eng*. **45** No 7, 1700 (2016) https://doi.org/10.1016/S1875-5372(16)30143-6.
13. D. Souad, S. Benramache, A. Ammari, A. Gahtar, *Iran. J. Phys. Res*. **22** No 3, 185 (2022) https://doi.org/10.47176/ijpr.22.3.01590.
14. Said Benramache, Yacine Aoun, *Ann. West Univ. Timisoara-Physics* **LXI**, 56 (2019) https://doi.org/10.2478/awutp-2019-0005.
15. Ratnawati, Jarnuzi Gunlazuardi, Slamet, *Mater. Chem. Phys*. **160**, 111 (2015) https://doi.org/10.1016/j.matchemphys.2015.04.013.
16. A. Gahtar, S. Benramache, B. Benhaoua, F. Chabane, *J Semicond*. **34** No 7, 073002 (2013) https://doi.org/10.1088/1674-4926/34/7/073002.
17. Y. Aoun, S. Benramache, B. Maaoui, A. Sbaihi, *J. Nano-Electron. Phys*. **16** No 1, 01023 (2024) https://doi.org/10.21272/jnep.16(1).01023.
18. A. Gahtar, S. Benramache, A. Ammari, A. Boukhachem. *Ann. West Univ. Timisoara-Phys*. **63** No 1, 1 (2021). https://doi.org/10.2478/awutp-2021-0001.
19. G. Surender, F.S. Omar, S. Bashir, M. Pershaanaa, S. Ramesh, K. Ramesh, *J. Energy Storage* **39**, 102599 (2021) https://doi.org/10.1016/j.est.2021.102599.
20. D. Govindarajaran, J. Selthraj. *NeuroQuantology* **20** No 17, 1350 (2022) https://doi.org/10.48047/NQ.2022.20.17.NQ880170.


## Високоякісні тонкі плівки $Co_3S_4$ з електропровідністю, отримані методом розпилювального піролізу


Abdelouahab Gahtar[1], Laid Dahbi[2], Chouaieb Zaouche[2], Said Benramache[3], Amira Sbaihi[3], Abdelghani Lakel[3], Okba Belahssen[3]

[1] *Department of Biology, Faculty of Sciences, University Elchahid Hamma Lakhder, 39000 El Oued, Algeria*
[2] *SALAMA Lab, Higher School of Saharan Agriculture – El Oued, PB 90 Chouhada, 39011 El-Oued, Algeria*
[3] *Laboratoire des Matériaux, des Énergies et de l'Environnement, University of Biskra 07000, Algeria*

У цьому дослідженні повідомляється про осадження тонких плівок сульфіду кобальту ($Co_3S_4$) на скляних підкладках за допомогою методу розпилювального піролізу за температури підкладки 350 ± 5 °C. Розчин-попередник був приготований з гексагідрату хлориду кобальту та тіосечовини, розчинених у бідистильованій воді, з додаванням невеликої кількості оцтової кислоти для підвищення розчинності та стабільності розчину. Структурні властивості осаджених плівок були досліджені за допомогою рентгеноструктурного аналізу, який підтвердив утворення полікристалічного $Co_3S_4$ з кубічною структурою шпінелі (Fd-3m). Плівки демонстрували переважну орієнтацію вздовж кристалографічної площини (113). Середній розмір кристалітів становив приблизно 13,4 нм, з розрахунковим параметром решітки 9,405 Å, що вказує на хорошу кристалічну якість. Оптична характеристика показала, що плівки мають ширину забороненої зони прямої оптичної зони 1,88 еВ, що свідчить про сильне поглинання у видимій області, що є перевагою для оптоелектронних застосувань. ІЧ-спектроскопія з перетворенням Фур'є підтвердила наявність характерних коливань зв'язку Co-S, що підтверджує успішне утворення сульфіду. Електричні вимірювання показали високу електропровідність близько $9{,}60 \times 10^{-1}$ (Ом·см)$^{-1}$, що вказує на квазіметалеву поведінку та ефективне перенесення заряду всередині плівки. Ці комбіновані структурні, оптичні та електричні властивості демонструють, що розпилювальний піроліз є простим, недорогим та ефективним методом отримання високоякісних тонких плівок Co3S4, що робить їх перспективними кандидатами для застосування в оптоелектронних пристроях, сенсорах та енергетичних технологіях.

**Ключові слова:** Сульфід кобальту, Розпилювальний піроліз, Рентгенівська дифракція (XRD), Інфрачервона спектроскопія з перетворенням Фур'є (FTIR), Електропровідність.